

# ASSESSMENT OF AIR POLLUTION BY AEROSOLS OVER A COAL OPEN-MINE INFLUENCED REGION IN SOUTHWESTERN ROMANIA

A. DUMITRU<sup>1</sup>, E.-A. OLARU<sup>2</sup>, M. DUMITRU<sup>3</sup>, G. IORGA<sup>1,4</sup>

<sup>1</sup> University of Bucharest, Faculty of Physics, Atomistilor 405, 077125 Bucharest-Magurele, Romania

<sup>2</sup> University of Bucharest, Faculty of Biology, Spl. Independentei 91–95, 050095 Bucharest, Romania

<sup>3</sup> National Institute for Laser, Plasma and Radiation Physics, Atomistilor 409,  
077125 Bucharest-Magurele, Romania

<sup>4</sup> University of Bucharest, Faculty of Chemistry, Regina Elisabeta 4–12, 030018 Bucharest, Romania  
*Email: gabriela.iorga@g.unibuc.ro*

*Received August 12, 2023*

**Abstract.** The mining activity in open-pit coal sites exerts a high pressure over the surrounding environment and on the health of people working and living nearby. Using data from a total of six field campaigns, this study aimed to capture the level of exploitation activities in the residential area close to the coal open-mine in terms of mass concentrations and total carbon fractions (TC) of ambient PM<sub>10</sub>, PM<sub>2.5</sub> samples. Sampling campaigns were performed between spring of 2018 and spring of 2020, covered both working (full time, part-time) and non-working days at the coal exploitation, and captured also the seasonal variations of different fractions of PM and of their carbonaceous fraction. Fine fraction was also analyzed based on the aerosol Angstrom exponent, determined from measurements of the aerosol scattering coefficient at 450 nm, 550 nm and 700 nm by a nephelometer. The mass concentrations of PM and TC showed significant variations from full time working days to non-working days. The air quality (AQ) level is determined by the air quality index (AQI) specific for PM<sub>10</sub>. *In situ* measurements clearly indicated that AQI<sub>local</sub> gives better image on the level of air pollution than the AQI<sub>estim</sub> from AQ monitoring stations in the region, closest to the Matasari site. Insights into the morphology and composition of particles were obtained by scanning electron microscopy (SEM) and energy dispersive X-ray (EDX/EDS) and Fourier transform infrared spectroscopy (FTIR) analyses. Major elements that were identified C, O, Si, Ca, K, S, Cu, Ni, Fe, Mg, Ti have both crustal and anthropogenic origin, in various proportions.

**Key words:** air quality, particulate matter, coal, open cast mining.

DOI: <https://doi.org/10.59277/RomJPhys.2024.69.801>

## 1. INTRODUCTION

The atmospheric particulate matter (PM) is receiving a great attention worldwide [1] because, in association with gaseous pollutants, is responsible for numerous adverse health effects (*e.g.*, [2–4]), as it can be inhaled (PM<sub>10</sub>, particles less than 10 μm), can enter deep into lungs (PM<sub>2.5</sub>, particles less than 2.5 μm) or can even be dissolved into the blood (PM<sub>0.1</sub>, particles less than 0.1 μm). Other studies indicate that the presence of transition metals in PM samples play a significant role in the health consequences due to prolonged exposure to atmospheric particles [5].

In addition, PM can impair the air quality and visibility, can soil and damage the monuments or acidify the water, or can perturb the Earth radiative balance contributing to climate changes [6–9].

A variety of sources of particles exists, either natural (sea salt, volcanoes, wildfires, etc.) or anthropogenic, including industrial, transportation or agricultural activities. Among industrial activities, the mining activity in open-pit coal sites is considered to put a high pressure over the surrounding environment and the health of people living nearby, according to United Nations Economic Commission for Europe [10]. Air pollution from activities in coal mines is mainly due to emissions of particulate matter and gases including carbon oxides (CO<sub>x</sub>), methane (CH<sub>4</sub>), sulfur dioxide (SO<sub>2</sub>), and oxides of nitrogen (NO<sub>x</sub>). Therefore, the air quality in areas surrounding a coal mine attracted attention in various regions worldwide, such as China (*e.g.* [11–13]), India (*e.g.* [14, 15]), Europe (*e.g.* [16, 17]), and USA (*e.g.* [18]). Because the spatial resolution of an air quality monitoring network is relatively low, at least in Romania, information about the air pollution over this type of area is gained mainly by remote monitoring using various instruments onboard of satellites (*e.g.* [19]) or using instruments onboard of aircrafts in specific field campaigns (*e.g.* [20]). However, the satellite or *in situ* observations using aircrafts have low resolution in time. Sometimes, interpolation data collected at ground observing stations are used in multi-model ensemble systems to provide short-range forecasts based, thus, on real-time observations (*e.g.* Copernicus Atmosphere Monitoring Service, CAMS). In certain situations, the differences between the values measured *in situ* and those predicted based on interpolations of the observations can be significant. Therefore, the capture of details of the air pollution at land surface is still a very challenging task, especially for areas with complex terrain.

One of such area with many open-pit mines for coal extraction (lignite mostly) is located in the southwest part of Romania in the coal field Jilt-Oltenia, BCJ (Fig. 1), close to the coal field Rovinari (BCR), where also operate important thermal power plants that use the extracted coal from the surrounding perimeter (*e.g.* Turceni, Rovinari) as fuel. The area is of high interest because the energy sector has strategic importance for Romania, in the light of emission reductions required by the EU acquis, the European Directive for large combustion plants 2001/80/EC that aims to improve air quality in EU countries and protect against health risks due to the air pollution, and the IED Directive 2010/75/EU on industrial emissions, which replaced the previous LCP Directive 2001/80/EC. Since 2010, there are very few available measurements performed in this area [19–22] and they are focused on NO<sub>2</sub>, SO<sub>2</sub>, H<sub>2</sub>CO or to the intercomparison of PM<sub>10</sub> samplers [23]. The study of Dandocsi *et al.* [24] suggests a presence of a large fraction of organics and ammonium sulfate in PM<sub>1</sub> samples in 2014 from Turceni area. Observations from satellite, aircraft and mobile DOAS instruments during AROMAT campaigns in 2014 and 2015 reported by Merlaud *et al.* [20] for Jiu Valley demonstrated that the

four power plants located here represent hot-spots of SO<sub>2</sub> and NO<sub>2</sub> emissions. One very recent study in the area by Florințescu-Gheorghe *et al.* [25] was focused on a different topic: allergies of patients in Oltenia area due to ragweed pollen. It has been found that [26–28] some correlations can be identified between biogenic pollutants and non-biological air pollutants (correlations higher than 0.3 for nitrogen oxides and volatile organic compounds and over 0.4 for PM<sub>10</sub> and PM<sub>2.5</sub>). None of previous researches were focused on details of PM particle sizes, chemical composition and morphology or to the quality of air that people living there breathe it. The present study is important also taking into account that in the area nearby Matasari more than 100000 people live in cities and communes.



Fig. 1 – Map showing location of the open-pit coal mines in southwestern Romania (upper image) with a zoom over the location indicating the positions of coal extraction (left, down). A higher zoom (right, down) over the region also shows the residential area where sampling has been performed.

Figure created using Google Earth.

Considering the aforementioned issues, the aim of this study was to capture the level of exploitation activities in the residential area close to the coal open-mine in terms of mass concentrations of atmospheric PM<sub>10</sub>, PM<sub>2.5</sub> samples and to estimate the air quality in this residential area. Seasonal variation was investigated for both PM<sub>x</sub> fractions, and total carbonaceous fraction (TC). The present study also reports for the first time, to our knowledge, details of morphology of PM samples in Matasari/BCJ area in Jiu Valley.

The paper structure is as follows: Section 2 describes the study area, the sampling strategy and the techniques used, followed by the experimental data. Section 3 presents and discusses the results, while the conclusion section ends the paper.

## 2. MATERIALS AND METHODS

### 2.1. STUDY AREA DESCRIPTION

Matasari (44.85°N, 23.09°E) is a small village on the Getic Plateau, in the southwestern Romania and has a population of a little over 5000 inhabitants according to a recent estimate of the Romanian National Institute of Statistics. The climate is temperate-continental, with föhn winds from 180° to 360° directions. Mixed forests of oak and beech grew in the area, there are pastures and meadows, and soil (luvisol and cambisol, <https://www.isric.org/>) is rich in lignite coal. Matasari is located in one of the most important coal field area, Jilt Basin, BCJ, where most of the population in the village and in the villages nearby traditionally works. The air is perceived as having an elevated level of pollution, as is briefly explained in the following. A large part of pollution comes from the specific coal mining activities: extraction (leading to direct emissions), filling and storage in deposits that determines, in 30–90 days from storage, supplemental emissions due to the oxidation process with the air [22]. Coal transportation activities to the large electricity producers in the area (thermal power plants of Rovinari and Turceni) increase the level of pollution. As a result, different types of mining activities (*e.g.*, drilling, coal crushing, loading/unloading, blasting, transport) generate various size ranges of PM. To all of this, the air suffers from the pollution coming from domestic activities, especially during cold season when people there use coal, wood, and gas for heating.

As a consequence, the air is burdened with a very complex mixture of fine particles of fly ash and particles containing crystalline and amorphous silicon dioxide SiO<sub>2</sub>, aluminum Al<sub>2</sub>O<sub>3</sub> and iron oxide Fe<sub>2</sub>O<sub>3</sub>, calcium oxide CaO, various emissions from traffic fleet and from the coal combustion: sulfur dioxide SO<sub>2</sub>, nitrogen dioxide NO<sub>2</sub>, carbon monoxide CO, methane CH<sub>4</sub>, ethane C<sub>2</sub>H<sub>4</sub>, and polycyclic aromatic hydrocarbons PAHs.

### 2.2. PM SAMPLING STRATEGY

First two sampling campaigns were performed during 10 successive days in April 2018 and during 5 successive days in January 2019 and covered different working levels at the coal exploitation (full time, part-time and non-working days). Additional campaigns in summer and autumn of 2019, in winter 2019–2020, and in spring of 2020 were performed to capture the seasonal variations of PM<sub>x</sub> fractions and of their total organic carbonaceous fractions.

The sampling was performed in a residential area at 10 m over the ground for 12 hours per day using two low-volume samplers (LVS), at 2.3 m<sup>3</sup>h<sup>-1</sup> flow rate

(substrate: quartz fiber filter) and an eight-stage low-pressure cascade impactor, at  $1.8 \text{ m}^3\text{h}^{-1}$  flow rate (size range  $0.06\text{--}16 \text{ }\mu\text{m}$  diameter; substrate: aluminum foil). For the identification of fine fraction, the nephelometer TSI model 3563 operated during the campaign in winter 2019 at 1-min resolution measuring the aerosol scattering coefficient at 450 nm, 550 nm and 700 nm. Nephelometer data was also hourly averaged.

The measurements of temperature ( $T$ , °C), relative humidity (RH,%), wind speed (WS,  $\text{m s}^{-1}$ ), wind direction (WD, Degree) and solar radiation (SR,  $\text{W m}^{-2}$ ) were acquired every minute by an automatic weather station, equipped with an piranometer CMP6; these values were then hourly averaged. Hourly estimates of the height of atmospheric mixing layer (MLH) were extracted from ERA5 reanalysis database of global climate variables produced by Copernicus Climate Change Service (C3S, [29]) at European Centre for Medium-Range Weather Forecasts.

### 2.3. EXPERIMENTAL METHODS AND DATA ANALYSIS

The PM mass concentrations were obtained by gravimetric analysis following the standard procedure in SR EN 12341:2002 and in SR EN 14907:2006. The quartz fiber filters (QF) were pre-weighed and pre-conditioned for at least 48 h at about  $20 \pm 1^\circ\text{C}$  and relative humidity of  $50 \pm 5\%$ , each filter being three times weighed. Results here are reported as averages of three weighings, both for the aerosol deposits on QF and on the Al foils.

Total carbon content in an aerosol sample [30] consists of an inorganic fraction and an organic one. Together with other co-emitted compounds, both carbon fractions are major components of soot, a carbonaceous substance generally resulted from the incomplete combustion of fossil fuels (coal, gasoline, diesel fuel, heating oil, wood, biomass and other agricultural waste, etc.). Consequently, it contains a large number of compounds. Various terms are used for different sub-fractions of total carbonaceous fraction of PM and some are often used interchangeably, although they are not the same, leading to terminological confusions. All details regarding the terminology and techniques associated to various fraction of the total carbon content of PM are thoroughly discussed in [31 and references therein].

Chemical analyses for soot or total carbon were performed by a procedure currently used in the field (*e.g.*, [32, 33]) namely, by taking punches of  $1.5 \text{ cm}^2$  from the QF filter, introducing them into the oven of HiperTOC analyzer coupled with a Non-Dispersive Infrared detector (Thermo Scientific) and analyzed following the procedure in Wang *et al.* [34], who also describe in detail the working mechanism of the device. TOC fraction can be then obtained by the analyzer as difference between inorganic carbon and total carbon. To further investigate the chemical composition of PM samples, to detect and quantify functional groups in atmospheric aerosols, giving insights for surface science, such as heterogeneous reactions analysis and for water adsorption on mineral oxides, Fourier transform infrared spectroscopy FTIR was involved (*e.g.*, [35, 36]). Information on the morphology of particles and elemental composition of ambient samples was obtained by scanning electron microscopy (SEM)

and energy dispersive X-ray (EDX/EDS) spectroscopy, powerful techniques [37] that have been used for a long time for the environmental samples [38–41]. Consequently, SEM, EDX/EDS and FTIR investigations were performed on quartz fiber filters and on selected size-resolved particulate matter samples collected in spring of 2018, corresponding to three days of different level of working activities at the mines: full time labor (three working shifts), labor reduced to a third (one working shift), and no activity period. Thermo Scientific™ Apreo SEM equipped with an Octane Elite Super Silicon Drift Detector (SDD) and TEAM™ EDS Analysis System and a Bruker Vertex 70 spectrometer with Helios ATR-accessory microscope were used to perform these measurements.

Additionally, daily mass concentrations of air pollutants PM<sub>10</sub>, PM<sub>2.5</sub>, NO<sub>2</sub>, O<sub>3</sub>, SO<sub>2</sub> were extracted from the National Air Quality database ([www.calitateaer.ro](http://www.calitateaer.ro)) for the stations closest to the point of interest (Tirgu-Jiu, Turceni, Rovinari, Drobeta Turnu Severin) in order to compare the air quality index (AQI<sub>estim</sub>) from the interpolated values with the AQI<sub>local</sub> calculated using the local measurements performed in current study using the rule of the scale from the National Monitoring AQ Network. The inverse Euclidean distance was used as interpolation method, currently used in the air quality field. Hourly data were converted to daily means, while PM mass concentrations of local samples were multiplied by 2 to cover the 24-h period.

### 3. RESULTS AND DISCUSSION

#### 3.1. PARTICULATE MATTER AND TOTAL CARBON VARIATIONS

Figure 2 shows the open-pit mine pollutes significantly the mine neighborhood. Both time series of PM<sub>2.5</sub> and PM<sub>10</sub> mass concentrations were very high for all seasons, with systematic exceedances of the air quality levels imposed by the EU limits. Pollution in the area is significantly higher than in the most polluted city in the Romania [41]. The lowest mean values of PM<sub>10</sub> (PM<sub>2.5</sub>) mass concentrations were measured during the summer field campaign (61 μg m<sup>-3</sup> and 44 μg m<sup>-3</sup>, respectively). Figure 2 also suggests the contribution of fine particles to PM<sub>10</sub> and the TC contribution to PM<sub>10</sub> and PM<sub>2.5</sub> fractions. On average per season, fine particles contribute from about 60% to the PM<sub>10</sub> in spring 2020 to 84% during winter season. To note that peaks in winter and spring 2020 correspond to an extremely high local pollution event (elevated local emissions combined with favorable meteorological condition: atmospheric calm, humid air, cold day and a very low atmospheric boundary layer height) and to the mixed Saharan and Asian dust intrusion event [42], respectively. Daily means of observed temperature T (°C), relative humidity RH (%), wind speed WS (m s<sup>-1</sup>) and MHL (m) together with air mass back trajectories using the HYSPLIT trajectory model were calculated for all field campaign and they support this conclusion but they are not shown here. During all field campaigns the meteorological conditions corresponded in general

to atmospheric stability, with very low or no precipitations. TC varies in  $PM_{10}$  samples from 8% in summer and early spring to 54% in winter, and from 4% in summer to 70% in winter in  $PM_{2.5}$  samples, suggesting the additional fresh soot resulting from coal combustion used for domestic heating in winter.

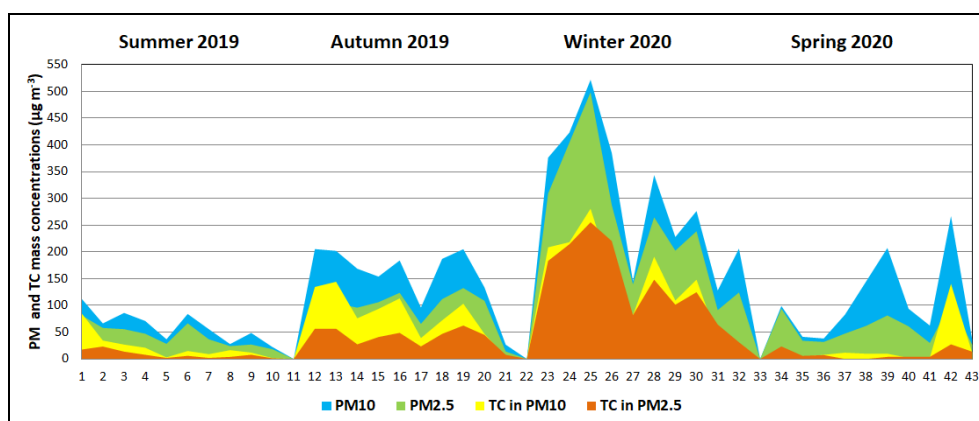


Fig. 2 – Time series of mass concentrations of  $PM_{10}$ ,  $PM_{2.5}$ , and TC during seasonal campaigns in 2019 and 2020.

In general, the average mass concentrations observed in this study were much smaller than those detected earlier in a coal mining area in India [14] or in Turkey [44] but much higher than those detected in Western Macedonia (North-western Greece), a region largely also dominated by lignite mining and lignite-fired power plants [17] or in Poland, in the vicinity of the Adamów coal-fired power plant [45] or in some small settlements close to opencast mines in the North-Bohemian Brown Coal Basin in Czech Republic [16]. However, similar levels of  $PM_{10}$  mass concentrations were measured at some sites in Appalachian region (USA), where environmental impacts of surface coal mining are also high and sampling there revealed  $PM_{10}$  levels as high as hundreds of  $\mu\text{g m}^{-3}$  [18]. Seasonal behavior is similar to that detected in Western Macedonia ([46] and references therein) and in contrast to that in Kozani, Greece [47], although a relative similarity between the topographic characteristics between the Matasari area and Kozani area exist. This could explain a part of the similarity of the elevated levels of  $PM_{10}$  measured in both locations. However, one notes that the heavy PM pollution in the area is more probably a result of a complex system of factors: local anthropogenic sources, resuspension, and mesoscale pollution transport.

### 3.2. CHARACTERISTICS OF LOCAL AIR POLLUTION: BEHAVIOR OF FINE AND COARSE PM AND TC FRACTIONS

Field campaigns in 2018 and 2019 allowed showing that the variations in the atmospheric mass concentrations reflected the varying operational activity in the

mine and that the anthropogenic activity strongly affects atmospheric pollution levels on daily timescales.

With respect to the air quality levels imposed by the EU, the field campaigns in 2019 and 2018 revealed that  $PM_{10}$  ( $PM_{2.5}$ ) mass concentrations comply with the AQ limits for both aerosol fractions after the third day after the cessation of the extraction activity. The daily mean values of  $PM_{10}$  and  $PM_{2.5}$  measured in this case in 2019 were about  $36 \mu\text{g m}^{-3}$  and  $18 \mu\text{g m}^{-3}$ , respectively. A decrease of the mining activity by up to a third seems to lead to an improvement of the air quality as  $PM_{10}$  and  $PM_{2.5}$  levels decreased up to  $41 \mu\text{g m}^{-3}$  and  $23 \mu\text{g m}^{-3}$ .

In summary, the sampling during 2018 campaigns shows a variation of the fine and coarse mass fractions as in the Fig. 3 (A). The mean  $PM_{2.5}/PM_{10}$  ratio has a value of 0.54 and varies between 0.38 on working days at maximum capacity (three shifts), increases on days when work is done at 1/3 of capacity (one shift) and reaches 0.63 on non-working days. We notice that the coarse aerosol is dominant in the days with maximum activity at the coal mine and decreases as the activity decreases. The fine fraction of aerosol is higher on the days when no work was done, and a maximum appear in the second non-working day (fourth sampling day on the graph), which may indicate the presence of aged fine aerosol in the atmosphere. However, the field campaign data in 2018 suggests TC varies as is preponderant in the coarse fraction.

This variation shows how in the atmosphere of the residential area where the measurements were carried out, the ratio fine particles *versus* coarse particles changes from the presence of predominant coarse particles in the atmosphere in full working days at the coal mine, up to its lowest level as mining activities are reduced and then stopped, when a fairly high mass of fine particles remains in the atmosphere. This remaining fine aerosol mass, when is favored by meteorological conditions (lack of precipitation and low wind speeds, high humidity, etc.) begins to suffer aging processes. The presence of coarse size aerosol in the atmosphere of the mine surrounding environment was also detected in earlier studies [48]. The fine and coarse fraction of PM was also investigated by measurements with the nephelometer. The results of sampling with the two types of instruments support and complement each other.

Total scattering coefficient in Fig. 4 (left) and frequency of occurrence of Angstrom coefficient in Fig. 4 (right) show that atmosphere in the residential sampling area is clearly influenced by the anthropogenic activity at the open-pit mines, as in the 5th day of strike the scattering coefficient decreases by an order of magnitude, from  $2.36\text{E-}04$  to  $5.87\text{E-}05$  (daily mean values at 550 nm) in the fifth sampling day of the field campaign in 2019. In the second sampling day, a contribution to the scattering process could come from some fine dust that was probable transported from medium distances, as meteorology data and the HYSPLIT air mass back trajectories indicated a southwest trajectory from Serbia and a very low atmospheric boundary layer. In the very early morning of this last sampling day

(inset of the Fig. 4 left) some snow (1 mm) also was present. Highest values of total scattering coefficient are observed in early morning and in late evening, in part due to increased relative humidity, when the multiple scattering processes became dominant in comparison with daytime between 10:00 and 17:00. A role could be also played by the fact that solar radiation comes at higher zenith angles as sunrise and sunset moments are approaching. The atmosphere loads every day with relatively constant fresh aerosol during the activity at mines; that loading decreases from 12th ( $AE_{450-700} = 1.64$ ) to 16th Jan ( $AE_{450-700} = 1.30$ ), in the fifth day of strike, with business as usual activity for the rest of everyday life of people during this period. We also notice the large presence of ultrafine ( $< 0.1 \mu\text{m}$ ) and fine particles (from  $0.1$  to  $1 \mu\text{m}$ ), in the accumulation mode (according to Kaufmann criterion). This result is also strengthened by the SEM/EDX analysis (see the example in Fig. 6) and by the magnetometry analysis [43].

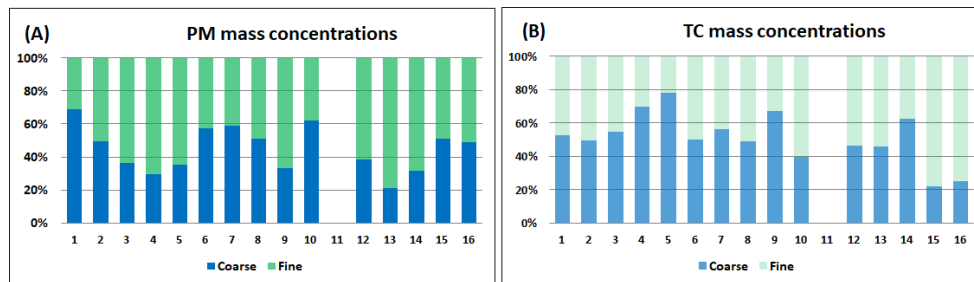


Fig. 3 – Daily percentages of fine  $PM_{2.5}$  and coarse  $PM_{10-PM_{2.5}}$  mass concentrations (A) and of TC content in fine and coarse PM fractions (B) for the field campaigns capturing various levels of mining activity (first 10 days) and during five consecutive days of strike (days from 12 to 16).

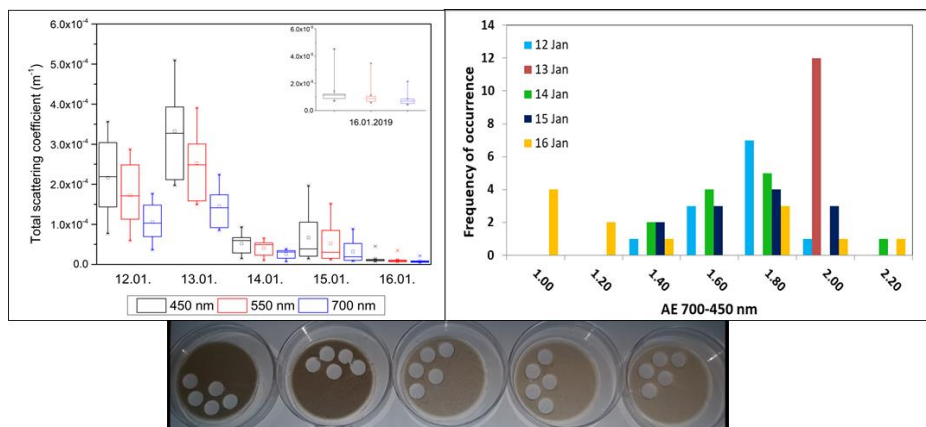


Fig. 4 – Total scattering coefficient measured by the nephelometer at 450 nm, 550 nm and 700 nm (upper left), frequency of occurrence of Angstrom coefficient calculated for the spectral interval 450–700 nm (upper right); picture of the samples (down) during the strike on January 2019.

The results regarding variation of aerosol particle levels in the Matasari atmosphere in 2018 and January 2019 were reinforced by the results of the subsequent campaigns in 2019 and 2020.

### 3.3. CHARACTERISTICS OF LOCAL AIR POLLUTION: AIR QUALITY INDEX

Severity of air pollution arising within the area was evaluated by the air quality index AQI ([www.calitateair.ro](http://www.calitateair.ro)). The comparison between air quality specific index  $AQI_{local}$  (based on *in situ* measured  $PM_{10}$ ) during all field campaigns in 2019–2020 and  $AQI_{estim}$ , calculated based on interpolated values from measurements at closest AQ monitoring stations for  $PM_{10}$ ,  $SO_2$ ,  $NO_2$ ,  $O_3$ , clearly indicates that air quality level is determined by the AQI specific for  $PM_{10}$ . Specific  $AQI_{estim}$  for gaseous species corresponded to AQ scale level 1 (good AQ) during all seasons, with the exception of  $O_3$ -specific  $AQI_{estim}$  during summer 2019 when the scale level 2 (satisfactory AQ) was obtained. The results for  $PM_{10}$ -specific both  $AQI_{local}$  and  $AQI_{estim}$  ranged from 1 (good AQ) to 6 (extremely poor) with better air quality during summer and spring (see also Fig. 2).  $AQI_{local}$  values indicated a higher pollution than that resulted from the estimation by interpolation: in 73% cases  $AQI_{local}/AQI_{estim}$  ratio varies between 1 and 2, and in over 80% cases  $AQI_{estim}$  underestimates the local pollution. Figure 5 shows frequencies of occurrence of air quality levels attributed by both  $AQI_{local}$  and  $AQI_{estim}$  (Fig. 5A), and the ratio of the  $AQI_{local}/AQI_{estim}$  (Fig. 5B).

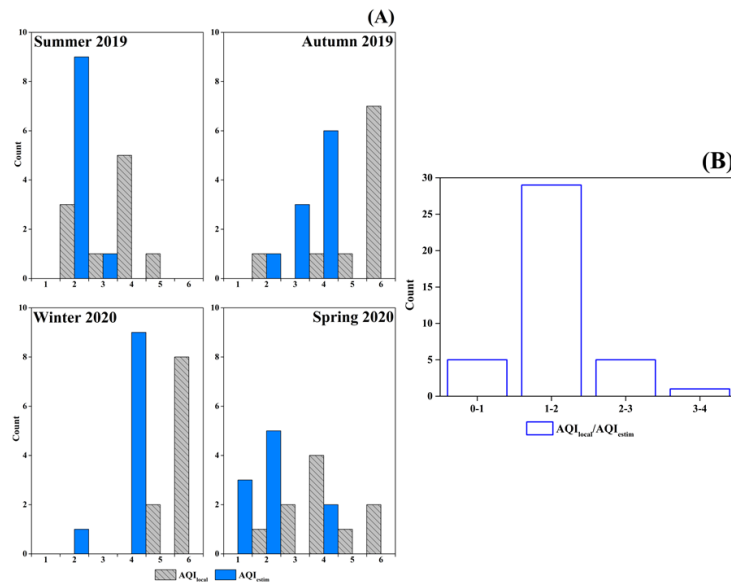


Fig. 5 – Comparison of AQI estimated from interpolated measurements at nearby stations ( $AQI_{estim}$ ) versus AQI calculated based on local PM measurements ( $AQI_{local}$ ): A) seasonal comparison ( $AQI_{estim}$ , blue bars and  $AQI_{local}$ , grey bars); B) ratio  $AQI_{local}/AQI_{estim}$ .

### 3.4. MORPHOLOGICAL AND CHEMICAL ANALYSIS

SEM complemented with EDS provided detailed information about particle size, chemical (elemental) composition and the surface morphology of aerosol particles. The morphological parameters, such as particle shape and diameter, were manually measured on images obtained for each sample. Further on, from the obtained EDS spectra, different peaks were identified and the percentage of weight of each element was calculated. SEM and EDS results of some selected samples during the studied period are shown in Fig. 6. Carbonaceous fraction in PM samples always contains organic compounds whose molecules contain carbon, oxygen, nitrogen and hydrogen. FTIR spectra of the selected size-resolved samples (sub- and super-micron size ranges) were presented in detail in [49]. Here only the main elements and functional groups based on the spectroscopy analysis that was applied to selected size-resolved particulate matter samples collected in spring of 2018 are synthesized.

Following the procedure proposed by Allen *et al.* (1994) and Ma *et al.* (2010) in [35, 36] we identified on the DRIFT spectra obtained in reflectance units and transformed using Kubelka-Munk function in absorbance units [50], some organic functional group and inorganic compounds were identified: aliphatic carbons (C-H stretching, 2915, 2848  $\text{cm}^{-1}$ ); carbonyl/carboxyl carbons (C=O stretching, 1600–1850  $\text{cm}^{-1}$ ); organonitrates (CONO<sub>2</sub>, 850, 1300, 1600  $\text{cm}^{-1}$ ), amine groups (H-N bending, 1425  $\text{cm}^{-1}$ ), sulfate SO<sub>4</sub>= (612–615, 1105  $\text{cm}^{-1}$ ) and copper ions (Cu-O stretching, 530  $\text{cm}^{-1}$ ), calcium sulfate CaSO<sub>4</sub> (671  $\text{cm}^{-1}$ ).

As some other small peaks at frequencies in 530–580  $\text{cm}^{-1}$  range were observed, it is possible the presence of hematite and magnetite (Fe-O stretching and bending mode vibration, respectively), as it was found in other samples in Matasari area [43]. Differences appeared to be size-interval dependent, as in other ambient samples collected with various LPIs [41, 50–53]. The recorded DRIFT spectra on Matasari samples [49] also showed and the presence of PM-bounded and adsorbed water on mineral particles. Although we had few spectra, this result is consistent with the more comprehensive analysis of Tsyro *et al.* (2005), who showed that water associated to particles constitutes 20–35% of the annual mean PM<sub>10</sub> and PM<sub>2.5</sub> mass concentrations in Europe [54], but in some cases the percentages could be even more (calculated water content is found to be about 75–80% in PM<sub>2.5</sub> at Vienna and Streithofen).

The general sequence of detected elements in particulate samples in Matasari was C, O, S, Si, Fe, Cu, Ni, Mg, K, Ca, Ti, Na, N. Aluminum signal was not possible to identify here because of the interference with the signal from de Al foil substrate but in a parallel study on QF filters significant Al peaks appeared frequently on the EDX spectrum. C and O were present in highest percentages.

The identified C along with K and S is the sign of soot particles that result from various combustion processes, including coal and wood burning and the emissions from the very old vehicle fleet that is used for transport. Many aggregated spherical carbonaceous particles were found in our samples as well as in other studies [41, 43, 55]. Huertas *et al.* (2012) characterized airborne PM<sub>10</sub> collected from the opencast coal region in northern Colombia and reported that the main elements present were are carbon, oxygen, potassium and silicon with average mass concentrations

of 41.5, 34.7, 11.6 and 5.7%, respectively [56]. Pandey *et al.* (2014) stated that the sequence of mean concentration of heavy metals from different sites in India is Fe > Cu > Zn > Mn > Pb > Cr > Cd > Ni [57]. Elemental analysis of PM<sub>10</sub> samples reported by Aneja *et al.* (2012) revealed the presence of Sb, As, Be, Cd, Cr, Co, Pb, Mn, Hg, Ni, Se [18], while Dubey *et al.* (2012) reported metal mean concentrations are found in the order of Fe > Cu > Zn > Mn > Cr > Cd > Pb > Ni [15].

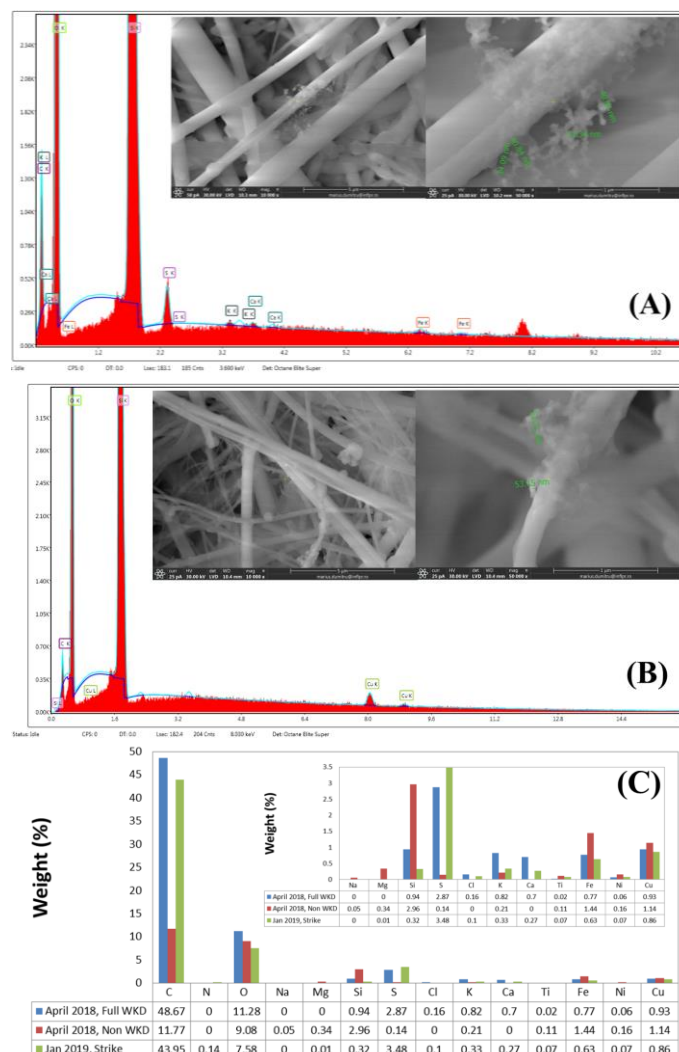


Fig. 6 – Examples of SEM micrographs of selected samples (Fig. 6A, B) and the atomic weight percentage of the elements identified by EDS (Fig. 6C) in April 2018 and 2019 campaigns (full WKD = full working days, non WKD = non-working days, Strike = strike days, all defined with respect to the extraction activity). The insets represent corresponding higher magnification images, highlighting the particle shapes and sizes and the weight of elements in smaller percentages.

Detected elements like Al, Si, O, Na, Ca, Fe, Mg, and K suggests the presence of natural particles, of irregular shapes, in form of aluminosilicates and quartz that could arise from the soil and road dust re-suspension due to wind or extraction plus transportation activities, as it was also identified in previous reports regarding open cast mining sites [58] or other environments [41, 59–61]. Based on these results, particulate matter was identified as of both anthropogenic (dominance of C, O, S, and presence of metallic elements like Co, Ti, Fe, Ni) and of natural crustal (geogenic particles showing abundance of Si, Al, Ca, Fe, Mg, Na) origins.

#### 4. CONCLUSIONS

Using data from a total of six field campaigns, this study captured the level of exploitation activities in the residential area close to a coal open-mine in terms of mass concentrations and total carbon fractions of ambient PM<sub>10</sub>, PM<sub>2.5</sub> samples. The total mass concentration of particulate matter samples showed significant variation from full time working days to non-working days, showing therefore PM<sub>10</sub>, PM<sub>2.5</sub> and TC levels from their background values to the highest. Seasonal variation was also shown. Coarse and fine fractions of aerosols in the residential area change depending on the intensity of the activities at the coal mine, in the sense that atmosphere is loaded with a higher coarse fraction when mining activity is at its highest level, and decrease up to a minimum when no significant coal extractions are performed, but the air remain loaded with a fine aerosol mass subjected to the aging process.

The air quality level is determined by the AQI specific for PM<sub>10</sub>. *In situ* measurements clearly indicated that AQI<sub>local</sub> gives a better image on the level of air pollution than the AQI<sub>estim</sub> from AQ monitoring stations in the region, closest to the Matasari site.

The findings by SEM, EDX, FTIR, DRIFT investigations matched and complemented each other. The general sequence of identified elements of both crustal and anthropogenic origin is C > O > S > Si > Fe > Cu > K > Ca > Mg > Ni > Ti > Na. SEM analysis showed both spherical particles and agglomerates of spherical particles, associated with anthropogenic sources and particles of irregular shapes, corresponding to natural, crustal origins.

Taking into account the location of Matasari and its climate characteristics, we suggest that the outcomes of present study provide useful insights on local air pollution that might be of help for authorities in taking air pollution mitigation measures in order to reduce the environmental stress on longer time scale.

*Acknowledgments.* AD and GI acknowledge the support from NO Grants 2014–2021, under Project EEA-RO-NO-2019-0423, contract no 31/01.09.2020. MD was supported by a grant of Ministry of Research, Innovation and Digitization, CCCDI-UEFISCDI, project number PN-III-P2-2.1-PED-2021-3678, within PNCDI III. Thanks to C. Herman for FTIR-DRIFT spectra performed on some PM

samples. European Center for Medium Range Weather Forecasts is acknowledged for providing the free access to ERA5 products (MLH) used in present study, <https://cds.climate.copernicus.eu/#!/search?text=ERA5&type=dataset> (last access: June 2022).

## REFERENCES

1. WHO, Billions of people still breathe unhealthy air: new WHO data, <https://www.who.int/news/item/04-04-2022-billions-of-people-still-breathe-unhealthy-air-new-who-data> (2022).
2. C.A. Pope, D.W. Dockery, *J. Air & Waste Manag. Assoc.* **56**, 709–742 (2006).
3. K. Bodor, Z. Bodor, A. Szep, R. Szep, *Sci. Rep.* **11**, 1–11 (2021).
4. K. Bodor, R. Szep, Z. Bodor, *Toxicol. Rep.* **9**, 556–562 (2022).
5. A.M. Florea, D. Buesselberg, *Biomaterials* **19**, 419–427 (2006).
6. S. Fuzzi, U. Baltensperger, K. Carslaw, S. Decesari, H. Denier Van Der Gon, M. C. Facchini *et al.*, *Atmos. Chem. Phys.* **15**, 8217–8299 (2005).
7. H.-Y. Liu, D. Dunea, S. Iordache, A. Pohoata, *Atmosphere* **9**, 150 (2018).
8. G.P. Bala, R. M. Rajnoveanu, E. Tudorache, R. Motisan, C. Oancea, *Environ. Sci. Pollut. Res.* **28**, 19615–19628 (2021).
9. J.H. Seinfeld and S.N. Pandis, *Atmospheric chemistry and physics. From air pollution to climate change*, 3rd Ed., Wiley-Interscience, New York, 2016.
10. United Nations Economic Commission for Europe (UNECE), [https://w3.unece.org/PXWeb/en/frPartyC140\\_27.05.2021\\_Annex7\\_rom.pdf](https://w3.unece.org/PXWeb/en/frPartyC140_27.05.2021_Annex7_rom.pdf) (2021).
11. W. Guo, M. Guo, Y. Tan, E. Bai, G. Zhao, *Sustainability* **11**, 4366 (2019).
12. Z. Wu, S. Lei, Q. Lu, Z. Bian, *Remote Sensing* **11**, 1820 (2019).
13. Y. Wang, X. Wu, S. He, R. Niu, *Nature Scientific Reports* **11**, 17549 (2021).
14. M.K. Goose, R.S. Majee, *J. Scientific & Industrial Research* **60**, 786–797 (2001).
15. B. Dubey, A.K. Pal, G. Singh, *Atmos. Poll. Res.* **3**, 238–246 (2012).
16. S. Hykysosva, J. Brejcha, *WIT Trans. Ecol. Environ.* **123**, 387–398 (2009).
17. V. Evagelopoulos, P. Begou, S. Zoras, *Atmosphere* **13**, 1900 (2022).
18. V.P. Aneja, A. Isherwood, P. Morgan, *Atmos. Environ.* **54**, 496–501 (2012).
19. D. Constantin, A. Merlaud, M. van Roozendaal, M. Voiculescu, C. Fayt, F. Hendrick, G. Pinardi, L. Georgescu, *Sensors* **13**, 3922–3940 (2013).
20. A. Merlaud, L. Belegante, D.-E. Constantin, M. den Hoed, A.C. Meier *et al.*, *Atmos. Meas. Tech.* **13**, 5513–5535 (2020).
21. G. Lazar, C. Capatina, C.M. Simonescu, *Rev. Chim. (Bucharest)* **65**, 11 (2014).
22. C. Capatina, D. Cirtina, *Rev. Chim. (Bucharest)* **68**, 2248–2255 (2017).
23. C. Nisulescu, D. Calinoiu, A. Timofte, A. Boscornea, C. Talianu, *Environ. Eng. Manag. J.* **10** (1), 99–105 (2011).
24. A. Dandocsi, A. Nemuc, C. Marin, S. Andrei, *Rev. Chim. (Bucharest)* **68** (4), 873–878 (2017).
25. N.A. Florincescu-Gheorghe, F. Popescu, D.O. Alexandru, F.D. Popescu, *Curr. Health Sci. J.* **45**, 66–72 (2019).
26. F. Oduber, A.I. Calvo, C. Blanco-Alegre, A. Castro, A.M. Vega-Maray, R.M. Valencia-Barrera, D. Fernandez-Gonzalez, R. Fraille, *Agric. For. Meteorol.* **264**, 16–26 (2019).
27. A. Rahman, C. Luo, M.H.R. Khan, J. Ke, V. Thilakanayaka, and S. Kumar, *Atmos. Environ.* **212**, 290–304 (2019).
28. A.M. Rosianu, P.M. Leru, S. Stefan, G. Iorga, L. Marmureanu, *Rom. Rep. Phys.* **74**, 703 (2022).
29. Copernicus Climate Change Service (C3S) at European Centre for Medium-Range Weather Forecast (<https://www.ecmwf.int/en/forecasts/dataset/ecmwf-reanalysis-v5>).
30. T. Novakov, *Sci. Total Environ.* **36**, 1–10 (1984).
31. D.A. Lack, H. Moosmüller, G.R. McMeeking, R.K. Chakrabarty, D. Baumgardner, *Anal. Bioanal. Chem.* **406**, 99–122 (2014).

32. B. J. Turpin, P. Saxena, E. Andrews, *Atmos. Environ.* **34**, 2983–3012 (2002).
33. S. Saarikoski, M. Sillanpa, M. Sofiev, H. Timonen, K. Saarnio, K. Teinila, A. Karppinen, J. Kukkonen, R. Hillamo, *Atmos. Environ.* **41**, 3577–3589 (2007).
34. J. Wang, L. Zhu, Y. Wahn, S. Gao, G. Daut, *Quarterly Internat.* **250**, 49–54 (2012).
35. D.T. Allen, E.J. Palen, M.I. Haimov, S.V. Hering, J.R. Young, *Aerosol Sci. Technol.* **21**, 325–342 (1994).
36. Q. Ma, H. He, Y. Liu, *J. Environ. Sci.* **22** (4), 555–560 (2010).
37. U.S. EPA: Guidelines for the Application of SEM/EDX Analytical Techniques to Particulate Matter Samples, EPA # 600/R-02/070 (2002).
38. J. Kasparian, E. Frejafon, P. Rambaldi, J. Yu, B. Vezin, J. P. Wolf, P. Ritter, P. Viscardi, *Atmos. Environ.* **32**, 2957–2967 (1998).
39. A. Campos-Ramos, A. Aragon-Pina, I. Galindo-Estrada, X. Querol, A. Alastuey, *Atmos. Environ.* **43**, 6159–6167 (2009).
40. F. Usman, B. Zeb, K. Alam, Z. Huang, A. Shah, I. Ahmad, S. Ullah, *Atmosphere* **13**, 124 (2022).
41. A. El-Taher, A. Ashry, A. Ene, M. Almeshari, H.M.H. Zakaly, *Rom. Rep. Phys.* **75**, 701 (2023).
42. G. Manolache, S. Stefan, G. Iorga, *Rom. J. Phys.* **64**, 808219 (2019).
43. A. Dumitru, C. Necula, M. Dumitru, G. Iorga, *Magnetic characterization of PM10 using non-linear Preisach maps. Toward domain state identification of magnetic anthropogenic particles*, under review (2023).
44. M. Onder, E. Yigit, *Environ. Monitor. Assess.* **152**(1–4), 393–401 (2008).
45. R. Cichowicz, G. Wielgosinski, A. Depta, *Int. J. Environ. Sci. Technol.* **17**, 3075–3086 (2020).
46. C. Samara, G. Argyropoulos, T. Grigoratos, A. Kouras, E. Manoli, S. Andreadou, C. Sahanidis, *Environ. Sci. Pollut. Res.* **25**(13), 12206–12221 (2017).
47. A.G. Triantafyllou, E.S. Kiros, V.G. Evagelopoulos, *J. Air Waste Manag. Assoc.* **52**, 287–296 (2002).
48. J. Saikia, P. Saikia, R. Boruah, B. K. Saikia, *Sci. Total Environ.* **530–531**, 304–313 (2015).
49. C. Herman, *Studiul analizei compoziționale a aerosolilor atmosferici într-o zonă aflată sub influența activității de exploatare minieră la suprafață*, Master Thesis (in Romanian), 2019.
50. Y.I. Tsai, S.-C. Kuo, *Atmos. Environ.* **40**, 1781–1793 (2006).
51. C. Coury, A.M. Dillner, *Atmos. Environ.* **43**, 940–948 (2009).
52. S. Takahama, A. Johnson, L. M. Russell, *Aerosol Sci. Tech.* **47**, 310–325 (2013).
53. N. Joshi, M.N. Romanias, V. Riffault, F. Thevenet, *Aeolian Research* **27**, 35–45 (2017).
54. S.G. Tsyro, *Atmos. Chem. Phys.* **5**, 515–532 (2005).
55. J. Wang, Z. Hu, Y. Chen, Z. Chen, S. Xu, *Atmos. Environ.* **68**, 221–229 (2013).
56. J. I. Huertas, M.E. Huertas, D.A. Soils, *Sci. Total Environ.* **423**, 39–46 (2012).
57. B. Pandey, M. Agrawal, S. Singh, *Atmos. Poll. Res.* **5**, 79–86 (2014).
58. D. P. Tripathy, T.R. Dash, *Arab. J. Geosci.* **12**, 514 (2019).
59. K. Teinila, V.-M. Kerminen, R. Hillamo, *J. Geophys. Res. Space Phys.* **105**, 3893–3904 (2000).
60. W. Li, L. Shao, Z. Wang, R. Shen, S. Yang, U. Tang, *J. Environ. Sci.* **22**, 561–569 (2010).
61. P.G. Satsangi, S. Yadav, *Int. J. Environ. Sci. Technol.* **11**, 217–232 (2014).